

# Entanglement Measurement Using Pump-Phase Control on an Up-Conversion Detector

K. F. Lee<sup>1</sup>, Paul Moraw<sup>1</sup>, D. R. Reilly<sup>1</sup>, and Gregory S. Kanter<sup>1</sup>

<sup>1</sup>NuCrypt, LLC, Park Ridge, IL 60068, USA

Author e-mail address: [kanterg@nucrypt.net](mailto:kanterg@nucrypt.net)

**Abstract:** We measure sequential time-bin entangled light by dynamically adjusting the pump phase of an up-conversion detector, allowing fast basis state control without adding loss to the quantum signal. © 2023 The Author(s)

The complete measurement of entangled photons requires measurements in many basis states. For polarization entangled photons the measured basis state is chosen by appropriate adjustment of polarization transformation devices, such as rotatable fixed waveplates [1] or variable waveplates [2]. Time-bin entanglement is commonly measured by interfering two temporal modes in a one-pulse delay asymmetric Mach-Zehnder interferometer (AMZI), which naturally creates three distinct time bins [3]. The early/late time bins form the “time” basis and measure each input mode independently, while the central time-bin forms the “energy” basis which is a coherent mixture of both modes. A complete measurement of time-bin entangled light measures in both the time and energy basis, where the energy basis must be measured with multiple coherent mixture phases. The phase of the coherent mixture is often controlled by changing the temperature of an integrated AMZI [3], which is inherently slow. In principle high speed phase modulators could be integrated into the AMZI, although this puts a constraint on the type of photonic circuit platform that can be used. Another option is to use a passive method, such as a 3x3 coupler, to simultaneously measure multiple phases [4], although such a scheme limits the available selectable phases.

Sequential time-bin entanglement [5] is similar to traditional time-bin entanglement, but is comprised of a constant rate of temporal bins, making every measurement through an AMZI dependent on the AMZI internal phase. While the time basis is no longer directly measurable, measurements like two-photon interference fringes (TPIs) can be recorded by appropriately changing the AMZI phases. This type of entanglement has been used for entanglement swapping over ~100 km [6], aided by a high 1 GHz pulse rate that is facilitated by the simplicity of the scheme.

We measure sequential time-bin TPI by first up-converting the signal/idler photons in a sum frequency generation (SFG) stage, then using AMZIs at the sum frequency to combine neighboring pulses. The TPI can be recorded by changing the phase of the AMZI using an internal piezo-electric transducer (PZT) stretcher, or it can be changed by using a high-speed phase modulator ( $\phi$ M) on the SFG pump. Since the phase of the pump is transferred to the sum frequency, the pump  $\phi$ M can also control the phase between sequential time bins thus controlling the measurement basis [7]. This allows fast control of the measurement basis without adding any lossy high speed phase shifters to the signal path. We believe this is the first time such a scheme has been used to measure entangled photons.

In addition to the enhanced measurement capability, placing the AMZI after the SFG stage allows both AMZI output ports to be detected by low-cost high-performance Silicon Single Photon Avalanche Detectors (SPADs). Since Silicon SPADs are lower-cost and higher-performing than their telecom-band III-V rivals, and because the SFG stage comprises much of the up-conversion detector (UCD) cost, the ability to detect both AMZI outputs using two Si SPADs with a single SFG stage reduces the relative cost of UCD in a host of applications, including quantum key distribution. We note that our experiment only uses one Si SPAD per AMZI due to a lack of available detectors, but both outputs are available.

The entangled source is shown in Figure 1 (a). A portion of an Acetylene gas line stabilized laser is split off to use as a frequency reference. The remainder is split into two arms with one arm being carved by an intensity modulator into 100 ps pulses at a 630 MHz rate, then amplified by an Erbium doped fiber amplifier (EDFA) to serve as a pump to a second harmonic generation (SHG) stage realized in a periodically poled lithium niobate (PPLN) waveguide. The resulting harmonic generated in the PPLN serves to produce photon pairs via spontaneous parametric down-conversion. Add drop multiplexers (ADMs) are used to separate signal and idler into wavelengths / bandwidths of 1539 / 1 nm and 1547.2 / 0.2 nm, respectively. The difference in bandwidth is due to equipment availability. The other arm propagates backwards through the same waveguide to create a continuous wave (CW) second harmonic reference frequency ( $SH_{ref}$ ).

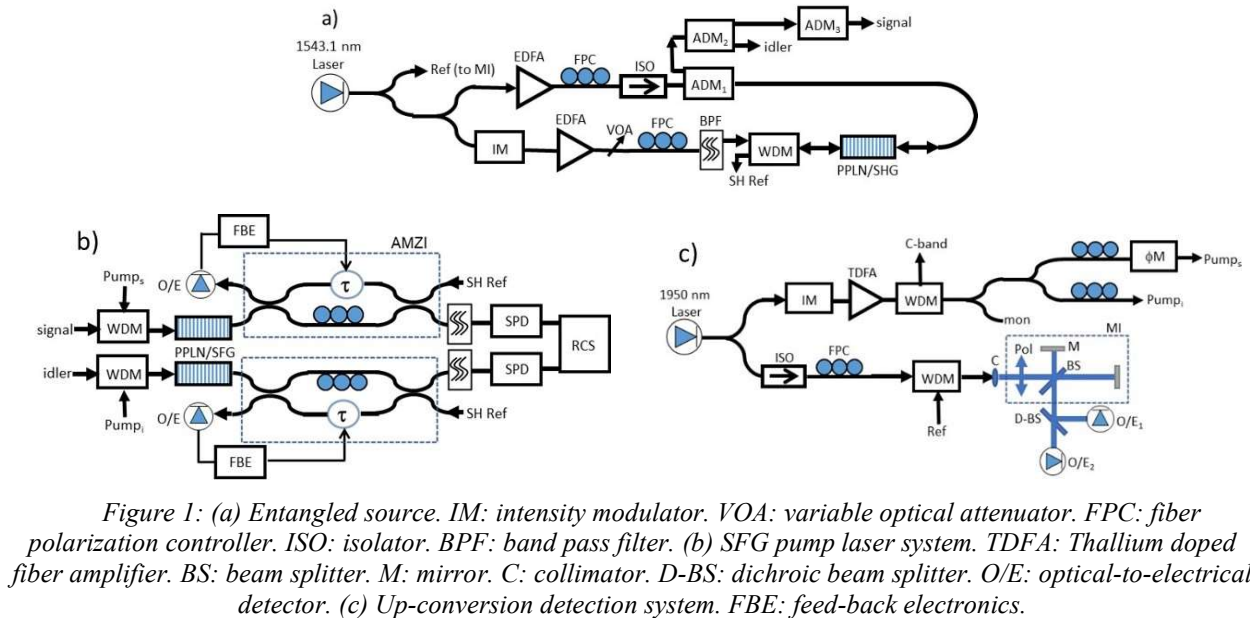
The UCD SFG pump at 1950 nm is carved into 500 ps pulses at a 630 MHz repetition rate and temporally aligned with the signals entering the SFG stage to up-convert them to about 860 nm. The sum frequency photons are filtered and detected in SPADs made by Excelitas Technologies. The net detection efficiency of the up-conversion detectors

(not including the sum frequency AMZI) is about 12% with a dark count probability per pulse of  $4 \cdot 10^{-6}$ . An all-fiber AMZI is constructed to interfere neighboring signal or idler pulses after the SFG, as shown in Figure 1 (b). Insertion of the AMZI after the SFG stage reduces the net detection efficiency due primarily to the  $\approx 60\%$  coupling efficiency from the waveguide to the single-mode fiber of the AMZI. The SFG pump at 1950 nm is frequency stabilized using a free-space Michelson interferometer (MI), as shown in Figure 1 (c). The MI uses a parabolic mirror collimator so that the 1950 nm laser and the 1543.1 nm reference signal, which are combined prior to the MI in a WDM, both interfere in the MI. The MI is stabilized to the reference signal using a PZT controlled mirror, and the 1950 nm pump laser is stabilized to the MI by varying the laser's temperature

The AMZI is phase-stabilized by measuring the backward-propagating  $SH_{ref}$  through the interferometer. The PZT stretcher is dithered and the resulting modulation of the  $SH_{ref}$  is analyzed to set the AMZI phase to a desired value. Note the harmonic reference is used instead of the fundamental so that the fiber splitters work reasonably well at both the sum frequency and  $SH_{ref}$  wavelengths. TPI fringes of the coincidence counts show a visibility of about 86% when one AMZI is scanned through a full  $360^\circ$  range with the other interferometer set to either  $0$  or  $90^\circ$ . The coincidence count rate of the fringe peak is 62 per 200 million pulses, with the singles count for the signal and idler being flat with respect to AMZI phase at  $3 \cdot 10^4$  or  $7 \cdot 10^3$  per 200 million pulses, respectively. The count rate difference between the detectors is in part due to a lossy filter in the idler arm that reduces its bandwidth to about 0.2 nm.

The detection system is then modified so that the basis measurement of the signal wavelength is determined by the SFG pump phase. The pump of the signal wavelength propagates through a phase modulator driven by a sinusoidal phase shift of 315 MHz. If the optical phase shift has a peak-to-peak value of  $\phi_{pp}$ , then the phase difference between consecutive up-converted pulses toggles between  $+\phi_{pp}$  and  $-\phi_{pp}$ . A variable attenuator on the RF phase modulation signal controls the phase-modulation depth and thus the value of  $\phi_{pp}$ . The detector data is received by post-processing electronics (NuCrypt Remote Correlation System or RCS) to separate these two measurements into different groups.

TPI fringes are recorded by setting the idler AMZI phase to  $0$  or  $90^\circ$  using the PZT, and changing  $\phi_{pp}$  on the signal AMZI to sweep out the correlation fringe. Figure 2 shows two non-orthogonal fringes with 83% average visibility. Each point represents  $10^9$  pulses. The main challenge recording TPI fringes with the AMZI after the UCD is the stability of fringe phase. This is in part due to the frequency stability of the UCD pump frequency which cause a corresponding change of the sum frequency thereby changing the effective phase-bias of the sum frequency AMZIs. This effect is ideally removed by frequency-locking the sum frequency pump to the Acetylene-stabilized laser via the MI, and allows the measurement seen in Figure 2 which is recorded over about one minute. However, various imperfections remain leaving some residual pump frequency drift.



A wavemeter (Thorlabs OSA203C) measured the net drift of the 1543.1 nm Acetylene-locked laser as  $\pm 5$  MHz over 15 minutes. Based on prior measurements beating the output from two independent lasers, we believe the laser stability is actually better and thus the measured frequency drift is likely limited by the wavemeter itself. The MI-stabilized pump wavelength was found to typically vary by  $\pm 10$  to  $\pm 20$  MHz over 15 minutes. The peak-to-peak drift

was thus several times greater than the Acetylene-locked laser, and the short-term variations were also noticeably higher. It seems this effect is due to imperfect frequency-locking of the pump to the 1543.1 nm laser via the MI. Given the 630 MHz AMZI free spectral range this level of frequency variation is manageable but not negligible. The unwanted frequency deviation could presumably be improved with more engineering effort. It also points to the advantage of using a more direct frequency stabilization scheme for the pump, such as using a wavemeter or gas-line.

A secondary reduction in stability is due to the sum-frequency AMZI's being individually stabilized to the sum frequency of the Acetylene-locked laser which is expected to vary in frequency by twice as much as the fundamental wavelength. This additional drift affects the accuracy of the PZT-set AMZI phases for a given fixed input signal frequency. Locking to a more stable laser or using an inherently stable thermally-tuned integrated photonic AMZI should reduce this effect. Additionally, we note that a shorter AMZI delay, or equivalently a higher pulse rate, would directly reduce the impact of frequency instability. The maximum pulse rate is inherently limited by the jitter of the detector,  $\tau_j$ , roughly to  $3 \cdot \tau_j$ , in order to clearly distinguish each pulse. The SPADs used here have a specified jitter of 400 ps, but other commercially available SPADs have much less jitter. For instance, the ID Quantique ID100 is rated at  $\tau_j = 40$  ps. This suggests operation at several GHz pulse rates, greatly increasing the tolerance to frequency drift.

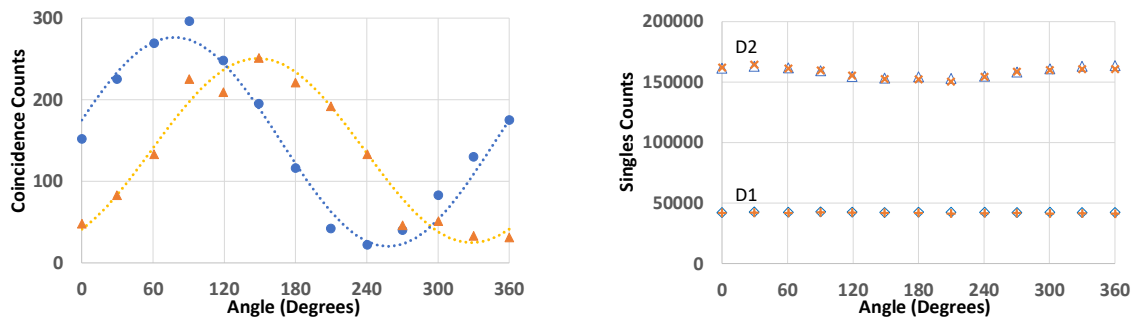


Figure 2: TPI measurement. (a) correlation TPI fringes. Curves are best fits to the data with corresponding visibility of 85.6% (blue dots) and 80.5% (orange triangles) (b) corresponding singles counts. D1 and D2 are two different detectors. Singles count data from either detector nearly overlaps for each fringe.

In summary, we have demonstrated the measurement of entangled photons using an UCD where the measurement basis is controlled by changing the pump phase. This design allows for fast control of the measurement basis without inserting additional lossy components in the quantum signal path, and since the AMZI is after the up-conversion process both AMZI outputs can be detected using just a single SFG stage with two low-cost Silicon single photon detectors. This shows the versatility of the UCD system and reduces the cost of up-conversion per detection port. We identified the issue of system stability due to various drifts including drift of the SFG pump wavelength, and noted means of further mitigating this issue in future designs.

**Acknowledgements:** This material is based upon work supported by the Defense Advanced Research Projects Agency (DARPA) and the Army Contracting Command-Aberdeen Proving Grounds (ACC-APG) under Contract No. W911NF-18-C-0053. The views, opinions, and/or findings are those of the authors and should not be interpreted as representing the official views or policies of the Department of Defense or the U.S. Government. Distribution Statement "A" (Approved for Public Release, Distribution Unlimited).

## References

- [1] J. B. Altepeter, Evan R. Jeffrey, and Paul G. Kwiat. "Photonic state tomography." *Advances in Atomic, Molecular, and Optical Physics* 52 (2005): 105-159.
- [2] S. X. Wang, *et al.*, "Fast Measurements of Entangled Photons," *Journal of Lightwave Technology*, vol. 31, no. 5, pp. 707-714, March 1, 2013, doi: 10.1109/JLT.2012.2231854.
- [3] H. Takesue and Yuita Noguchi. "Implementation of quantum state tomography for time-bin entangled photon pairs." *Optics express* 17.13 (2009): 10976-10989.
- [4] Wang, S. X., *et al.* "High-speed tomography of time-bin-entangled photons using a single-measurement setting." *Physical Review A* 86.4 (2012): 042122.
- [5] H. De Riedmatten, *et al.* "Tailoring photonic entanglement in high-dimensional Hilbert spaces." *Physical Review A* 69, no. 5 (2004): 050304.
- [6] Sun, Qi-Chao, *et al.* "Entanglement swapping over 100 km optical fiber with independent entangled photon-pair sources." *Optica* 4.10 (2017): 1214-1218.
- [7] K. F. Lee, *et al.* "Emulation of up-conversion based quantum key distribution scheme using active pump-controlled basis selection and adaptive thresholding." *Optics Communications* 475 (2020): 126258.